Thermal Stress and Deformation in Functionally Graded Material Shells of Revolution under Thermal Loading due to Fluid*

Shigeo TAKEZONO**, Katsumi TAO**
Eijiroh INAMURA** and Masahiro INOUE***

This paper is concerned with an analytical formulation and a numerical solution of the thermal stress and deformation for axisymmetrical shells of functionally graded material (FGM) subjected to thermal loading due to fluid. The temperature distribution through the thickness is assumed to be a curve of high order, and the temperature field in the shell is determined using the equations of heat conduction and heat transfer. The equations of equilibrium and the relationships between the strains and displacements are derived from the Sanders elastic shell theory. The fundamental equations derived are numerically solved using the finite difference method. As numerical examples, functionally graded cylindrical shells composed of SUS 304 and ZrO_2 subjected to thermal loads due to fluid are analyzed. Numerical computations are carried out for various compositional distribution profiles in FGM. The results show that the present method gives correct temperature distributions and that the temperature distributions, stress distributions and deformations vary significantly depending on these compositional distribution profiles.

Key Words: Structural Analysis, Thermal Stress, Functionally Graded Materials, Finite Difference Method, Thin Shells, Heat Conduction

1. Introduction

In recent years a functionally graded material (FGM) has been developed due to its excellent mechanical and thermal properties. For thermal stress relaxation analysis of structural components and/or mechanical components of FGM, many investigations have been carried out. These investigations, however, are almost limited to the simple geometries such as plates, hollow cylinders and hollow spheres[1]-[9]. Moreover they are almost all treated as multilayered composite models in spite of continuity of FGM and each layer is considered to be homogeneous[5]-[9].

In this paper the authors develop an analytical method for thermal deformation of FGM shells of revolution under thermal loading due to fluid. Material parameters are given by functions of the shell thickness direction, and each coefficient of basic equations related to material properties is determined from numerical integration through shell thickness. In order to improve the accuracy of the solutions for initial thermal loading stage, the temperature distribution through the thickness is supposed to be a curve of high order, and is determined using the equations of heat conduction and heat transfer. Suitable degree of temperature distribution polynomial is determined from evaluation of convergency of the solutions according to variation of the degree. Then using the obtained temperature distribution, the stresses and deformations are derived from the thermal stress equations. The equations of equilibrium and the strain displacement relations are derived from the Sanders thin shell theory[10]. The fundamental equations derived are numerically solved by the finite difference method in both space and time, and the

* Received 15th July, 1996. Japanese original: Trans. Jpn. Soc. Mech. Eng., Vol. 62, No. 594, A (1996), pp. 474-481 (Received 3rd July, 1995)
** Department of Mechanical Engineering, Toyohashi University of Technology, Tempaku-cho, Toyohashi 441, Japan
*** Nippon Sharyo Co. Ltd., Sanbonmatsu-cho, Atsuta-ku, Nagoya 456-91, Japan

solutions are obtained by integration of the incremental values.

As numerical examples, functionally graded cylindrical shells composed of SUS 304 and ZrO_2 subjected to thermal loads due to fluid, which are expressed by step function in regard of time, are analyzed. First we analyze the heat conduction problem of the long shell under axisymmetric thermal loading. The obtained temperature distributions are compared with ones obtained by other methods[9], and the accuracy of the solutions is evaluated. Secondly we analyze the simply supported cylindrical shells subjected to locally distributed axisymmetric thermal loading, and compare the solutions for various compositional distribution profiles in FGM.

2. Fundamental Equations

If the middle surface of axisymmetrical shells is given by $R=R(s)$, where R is the distance from the axis and s is the meridional distance measured from a boundary along the middle surface, the relations among the nondimensional curvatures ω_ξ $(=a/R_s)$, ω_θ $(=a/R_\theta)$ and the nondimensional radius r $(=R/a)$ become

$$\left.\begin{aligned} &\omega_\xi=-(\gamma'+\gamma^2)/\omega_\theta,\ \omega_\theta=\sqrt{1-(r')^2}/r,\\ &\omega_\theta'=\gamma(\omega_\xi-\omega_\theta)\quad r''/r=-\omega_\xi\omega_\theta,\\ &\gamma=r'/r,\ \xi=s/a,\ (\ )'=d(\ )/d\xi \end{aligned}\right\} \qquad (1)$$

where a is the reference length. An arbitrary point in the shell can be expressed in the orthogonal coordinate system (ξ, θ, ζ) as shown in Fig. 1.

2.1 Heat conduction equations

The equation of heat conduction at a point in the shell body, whose material parameters vary only along the shell thickness direction, is given in the orthogonal coordinates (ξ, θ, ζ) as

$$\frac{\partial T}{\partial t}-\frac{\chi}{a^2}\left\{\frac{1}{r}\frac{\partial}{\partial\xi}\left(r\frac{\partial T}{\partial\xi}\right)+\frac{1}{r^2}\frac{\partial^2 T}{\partial\theta^2}\right\} -\frac{1}{c\rho}\frac{\partial}{\partial\zeta}\left(\lambda\frac{\partial T}{\partial\zeta}\right)-\frac{\eta}{c\rho}=0 \qquad (2)$$

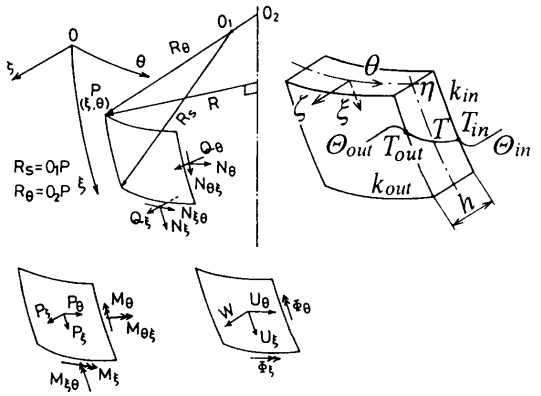

Fig. 1 Coordinates and notations

where T is the temperature at (ξ, θ, ζ, t), χ $(=\lambda/(c\rho))$ is the thermal diffusivity, c is the specific heat, ρ is the mass density, λ is the coefficient of thermal conductivity, η is the heat generation per unit volume and per unit time, and t is time.

The boundary conditions of the temperature on the inner and outer surfaces $(\zeta=\mp h/2)$ of the shell are

$$\left.\begin{aligned} &\left[\frac{\partial T}{\partial\zeta}\right]_{\zeta=-h/2}=k_{\text{in}}(T_{\text{in}}-\Theta_{\text{in}}),\\ &\left[\frac{\partial T}{\partial\zeta}\right]_{\zeta=h/2}=-k_{\text{out}}(T_{\text{out}}-\Theta_{\text{out}}) \end{aligned}\right\} \qquad (3)$$

where $k_{\text{in}}=K_{\text{in}}/(\lambda)_{\text{in}}$, $k_{\text{out}}=K_{\text{out}}/(\lambda)_{\text{out}}$ and K is the heat transfer coefficient. T_{in} and T_{out} are the temperatures on the inner and outer surfaces of the shell, Θ_{in} and Θ_{out} are ambient fluid temperatures of the shell, and h is the thickness of the shell.

The authors have analyzed the thermal conduction problems and thermal stress ones of homogeneous shells [11),(12)] and multi-layered ones[13]. In these studies the temperature distributions through the thickness have been assumed to be linear or a curve of the second order, and the temperature field in the shell has been determined (Only in the case of multi-layered thin shells, linear temperature distribution is adopted in each layer[13]). For the shells of functionally graded material, however, the temperature distribution in the initial response can not be estimated with enough accuracy by a curve of the low order, because the heat-resisting material component has the relatively small coefficient of thermal conductivity. In the present paper, to improve the accuracy of the solutions, the temperature distribution through the thickness is assumed to be a curve of p-th degree by using coefficients T_j $(j=0, 1, 2, \cdots, p)$ as follows:

$$T(\xi, \theta, \zeta, t)=\sum_{j=0}^{p} T_j(\xi, \theta, t)\zeta^j \qquad (4)$$

After substituting Eq. (4) into Eq. (2), integrating Eq. (2) multiplied by ζ^i $(i=0, 1, 2, \cdots, p)$ through the thickness, we obtain the following $(p+1)$ equations.

$$\left.\begin{aligned} &\frac{\partial}{\partial t}\int_{-h/2}^{h/2}\zeta^i\sum_{j=0}^{p}T_j\zeta^j d\zeta\\ &-\frac{1}{a^2}\left\{\frac{1}{r}\frac{\partial}{\partial\xi}\left(r\frac{\partial}{\partial\xi}\int_{-h/2}^{h/2}\zeta^i\chi\sum_{j=0}^{p}T_j\zeta^j d\zeta\right)\right.\\ &\left.+\frac{1}{r^2}\frac{\partial^2}{\partial\theta^2}\int_{-h/2}^{h/2}\zeta^i\chi\sum_{j=0}^{p}T_j\zeta^j d\zeta\right\}\\ &-\int_{-h/2}^{h/2}\zeta^i\frac{1}{c\rho}\frac{\partial}{\partial\zeta}\left(\lambda\frac{\partial}{\partial\zeta}\sum_{j=0}^{p}T_j\zeta^j\right)d\zeta\\ &-\int_{-h/2}^{h/2}\zeta^i\frac{\eta}{c\rho}d\zeta=0\quad (i=0, 1, 2, \cdots, p) \end{aligned}\right\} \qquad (5)$$

With consideration of the surface boundary conditions (Eqs. (3)), Eqs. (5) become as follows:

$$\left.\begin{aligned}&\sum_{j=0}^{p}\Big[\alpha_{(i,j)}\frac{\partial T_j}{\partial t}-\frac{\beta_{(i,j)}}{a^2}\Big(\gamma\frac{\partial T_j}{\partial\xi}+\frac{\partial^2 T_j}{\partial\xi^2}+\frac{1}{r^2}\frac{\partial^2 T_j}{\partial\theta^2}\Big)\\&-(\gamma_{(i,j)}+\delta_{(i,j)}+\varepsilon_{(i,j)}T_j\Big]-(\chi)_{\rm out}\Big(\frac{h}{2}\Big)^i k_{\rm out}\Theta_{\rm out}\\&-(\chi)_{\rm in}\Big(-\frac{h}{2}\Big)^i k_{\rm in}\Theta_{\rm in}-Q_i=0\quad(i=0,1,2,\cdots,p)\end{aligned}\right\}\tag{6}$$

where

$$\left.\begin{aligned}&\alpha_{(i,j)}=\frac{1+(-1)^{i+j}}{i+j+1}\Big(\frac{h}{2}\Big)^{i+j+1},\ \beta_{(i,j)}=\int_{-h/2}^{h/2}\chi\zeta^{i+j}d\zeta\\&\gamma_{(i,j)}=-(\chi)_{\rm out}\Big(\frac{h}{2}\Big)^{i+j}k_{\rm out}-(\chi)_{\rm in}\Big(-\frac{h}{2}\Big)^{i+j}k_{\rm in}\\&\delta_{(i,j)}=\Big\{\Big(\frac{1}{c\rho}\frac{\partial\lambda}{\partial\zeta}\Big)_{\rm out}\Big(\frac{h}{2}\Big)^i-\Big(\frac{\partial(\chi\zeta^i)}{\partial\zeta}\Big)_{\rm out}\Big\}\Big(\frac{h}{2}\Big)^j\\&\quad-\Big\{\Big(\frac{1}{c\rho}\frac{\partial\lambda}{\partial\zeta}\Big)_{\rm in}\Big(-\frac{h}{2}\Big)^i-\Big(\frac{\partial(\chi\zeta^i)}{\partial\zeta}\Big)_{\rm in}\Big\}\Big(-\frac{h}{2}\Big)^j\\&\varepsilon_{(i,j)}=\int_{-h/2}^{h/2}\Big\{\frac{\partial^2(\chi\zeta^i)}{\partial\zeta^2}-\frac{\partial}{\partial\zeta}\Big(\frac{\zeta^i}{c\rho}\frac{\partial\lambda}{\partial\zeta}\Big)\Big\}\zeta^j d\zeta\end{aligned}\right\}\tag{7}$$

$$Q_i=\int_{-h/2}^{h/2}\frac{\eta}{c\rho}\zeta^i d\zeta\tag{8}$$

For $(p+1)$ independent variables T_j $(j=0, 1, 2, \cdots, p)$, Eqs.(6) are given, and by solving these equations, the temperature field in the shell can be determined.

2.2 Thermal deformation equations

Eliminating the transverse shear forces Q_ξ and Q_θ in the equilibrium equations in the Sanders theory[10], and expressing in the differential form with time or load, the following equations are obtained.

$$\left.\begin{aligned}&a\Big[\frac{\partial}{\partial\xi}(r\dot N_\xi)+\frac{\partial}{\partial\theta}(\dot{\bar N}_{\xi\theta})-r'\dot N_\theta\Big]\\&\quad+\omega_\xi\Big[\frac{\partial}{\partial\xi}(r\dot M_\xi)+\frac{\partial}{\partial\theta}(\dot{\bar M}_{\xi\theta})-r'\dot M_\theta\Big]\\&\quad+\frac{1}{2}(\omega_\xi-\omega_\theta)\frac{\partial}{\partial\theta}(\dot{\bar M}_{\xi\theta})+ra^2\dot P_\xi=0\\&a\Big[\frac{\partial}{\partial\theta}(\dot N_\theta)+\frac{\partial}{\partial\xi}(r\dot{\bar N}_{\xi\theta})+r'\dot{\bar N}_{\xi\theta}\Big]\\&\quad+\omega_\theta\Big[\frac{\partial}{\partial\theta}(\dot M_\theta)+\frac{\partial}{\partial\xi}(r\dot{\bar M}_{\xi\theta})+r'\dot{\bar M}_{\xi\theta}\Big]\\&\quad+\frac{1}{2}r\frac{\partial}{\partial\xi}\Big[(\omega_\theta-\omega_\xi)\dot{\bar M}_{\xi\theta}\Big]+ra^2\dot P_\theta=0\\&\frac{\partial}{\partial\xi}\Big[\frac{\partial}{\partial\xi}(r\dot M_\xi)+\frac{\partial}{\partial\theta}(\dot{\bar M}_{\xi\theta})-r'\dot M_\theta\Big]\\&\quad+\frac{1}{r}\frac{\partial}{\partial\theta}\Big[\frac{\partial}{\partial\theta}(\dot M_\theta)+\frac{\partial}{\partial\xi}(r\dot{\bar M}_{\xi\theta})+r'\dot{\bar M}_{\xi\theta}\Big]\\&\quad-ra(\omega_\xi\dot N_\xi+\omega_\theta\dot N_\theta)+ra^2\dot P_\zeta=0\end{aligned}\right\}\tag{9}$$

where $\dot{\bar N}_{\xi\theta}$ and $\dot{\bar M}_{\xi\theta}$ are the modified stress resultant and modified stress couple, respectively, and are expressed as follows[10]:

$$\left.\begin{aligned}&\dot{\bar N}_{\xi\theta}=(\dot N_{\xi\theta}+\dot N_{\theta\xi})/2\\&\quad+[(1/R_\theta)-(1/R_s)](\dot M_{\xi\theta}-\dot M_{\theta\xi})/4\\&\dot{\bar M}_{\xi\theta}=(\dot M_{\xi\theta}+\dot M_{\theta\xi})/2\end{aligned}\right\}\tag{10}$$

The other notations are shown in Fig. 1.

The strain rates of the middle surface are given by:

$$\left.\begin{aligned}&\dot\varepsilon_{\xi m}=\frac{1}{a}\Big[\frac{\partial}{\partial\xi}(\dot U_\xi)+\omega_\xi\dot W\Big]\\&\dot\varepsilon_{\theta m}=\frac{1}{a}\Big[\frac{1}{r}\frac{\partial}{\partial\theta}(\dot U_\theta)+\gamma\dot U_\xi+\omega_\theta\dot W\Big]\\&\dot\varepsilon_{\xi\theta m}=\frac{1}{2a}\Big[\frac{1}{r}\frac{\partial}{\partial\theta}(\dot U_\xi)+\frac{\partial}{\partial\xi}(\dot U_\theta)-\gamma\dot U_\theta\Big]\end{aligned}\right\}\tag{11}$$

where $\dot\varepsilon_{\xi\theta m}$ is half the usual engineering shear strain rate. The bending distortion rates $\dot\varkappa_\xi$, $\dot\varkappa_\theta$ and $\dot\varkappa_{\xi\theta}$ are as follows:

$$\left.\begin{aligned}&\dot\varkappa_\xi=\frac{1}{a}\frac{\partial}{\partial\xi}(\dot\Phi_\xi),\ \dot\varkappa_\theta=\frac{1}{a}\Big\{\frac{1}{r}\frac{\partial}{\partial\theta}(\dot\Phi_\theta)+\gamma\dot\Phi_\xi\Big\}\\&\dot\varkappa_{\xi\theta}=\frac{1}{2a}\Big[\frac{1}{r}\frac{\partial}{\partial\theta}(\dot\Phi_\xi)+\frac{\partial}{\partial\xi}(\dot\Phi_\theta)-\gamma\dot\Phi_\theta\\&\quad+\frac{1}{2a}(\omega_\xi-\omega_\theta)\Big\{\frac{1}{r}\frac{\partial}{\partial\theta}(\dot U_\xi)-\frac{\partial}{\partial\xi}(\dot U_\theta)-\gamma\dot U_\theta\Big\}\Big]\end{aligned}\right\}\tag{12}$$

where rotation rates $\dot\Phi_\xi$ and $\dot\Phi_\theta$ are:

$$\left.\begin{aligned}&\dot\Phi_\xi=\frac{1}{a}\Big[-\frac{\partial}{\partial\xi}(\dot W)+\omega_\xi\dot U_\xi\Big]\\&\dot\Phi_\theta=\frac{1}{a}\Big[-\frac{1}{r}\frac{\partial}{\partial\theta}(\dot W)+\omega_\theta\dot U_\theta\Big]\end{aligned}\right\}\tag{13}$$

Under the Kirchhoff-Love hypothesis and the neglect of quantities ζ/R_s and ζ/R_θ which are small in comparison with unity, the strain rates at the distance ζ from the middle surface are

$$\{\dot\varepsilon\}=\{\dot\varepsilon_m\}+\zeta\{\dot\varkappa\}\tag{14}$$

where

$$\left.\begin{aligned}&\{\dot\varepsilon\}=\{\dot\varepsilon_\xi,\ \dot\varepsilon_\theta,\ \dot\varepsilon_{\xi\theta}\}^T,\ \{\dot\varepsilon_m\}=\{\dot\varepsilon_{\xi m},\ \dot\varepsilon_{\theta m},\ \dot\varepsilon_{\xi\theta m}\}^T\\&\{\dot\varkappa\}=\{\dot\varkappa_\xi,\ \dot\varkappa_\theta,\ \dot\varkappa_{\xi\theta}\}^T\end{aligned}\right\}\tag{15}$$

and $\{\ \}^T$ represents the transposed matrix.

Using Eqs.(14), the stress rates in the plane stress state are written as

$$\{\dot\sigma\}=[D](\{\dot\varepsilon_m\}+\zeta\{\dot\varkappa\})-\{\dot\sigma^t\}\tag{16}$$

where

$$\left.\begin{aligned}&\{\dot\sigma\}=\{\dot\sigma_\xi,\ \dot\sigma_\theta,\ \dot\sigma_{\xi\theta}\}^T\\&\{\dot\sigma^t\}=\{\dot\sigma^t,\ \dot\sigma^t,\ 0\}^T=\frac{aE}{1-\nu}\{\dot T_e,\ \dot T_e,\ 0\}^T\\&[D]=\frac{E}{1-\nu^2}\begin{bmatrix}1&\nu&0\\\nu&1&0\\0&0&1-\nu\end{bmatrix}\end{aligned}\right\}\tag{17}$$

E, ν and α are Young's modulus, Poisson's ratio, and thermal expansion coefficient, and T_e is the temperature rise from the original temperature $\bar T_0$ to the present temperature T, namely,

$$T_e(\xi,\theta,\zeta,t)=T(\xi,\theta,\zeta,t)-\bar T_0\tag{18}$$

The membrane forces $\{N\}$ and the resultant moments $\{M\}$ per unit length are obtained from Eqs.(16):

$$\begin{aligned}\begin{Bmatrix}\dot N\\\dot M\end{Bmatrix}&=\{\dot N_\xi,\ \dot N_\theta,\ \dot{\bar N}_{\xi\theta},\ \dot M_\xi,\ \dot M_\theta,\ \dot{\bar M}_{\xi\theta}\}^T\\&=\int_{-h/2}^{h/2}\begin{Bmatrix}\dot\sigma\\\dot\sigma\zeta\end{Bmatrix}d\zeta\\&=\begin{bmatrix}\bar A&\bar B\\\bar B&\bar C\end{bmatrix}\begin{Bmatrix}\dot\varepsilon_m\\\dot\varkappa\end{Bmatrix}-\begin{Bmatrix}\dot N^t\\\dot M^t\end{Bmatrix}\end{aligned}\tag{19}$$

In Eqs.(19), $(\ )^t$ denotes the internal forces due to

temperature rise T_e and are given by

$$\left.\begin{aligned}\{\dot{N}^t\}&=\{\dot{N}^t, \dot{N}^t, 0\}^T=\int_{-h/2}^{h/2}\{\dot{\sigma}^t\}d\zeta\\ \{\dot{M}^t\}&=\{\dot{M}^t, \dot{M}^t, 0\}^T=\int_{-h/2}^{h/2}\{\dot{\sigma}^t\}\zeta d\zeta\end{aligned}\right\} \tag{20}$$

and $\bar{A}\sim\bar{C}$ are as follows:

$$\left.\begin{aligned}\bar{A}&=\int_{-h/2}^{h/2}[D]d\zeta,\ \bar{B}=\int_{-h/2}^{h/2}[D]\zeta d\zeta\\ \bar{C}&=\int_{-h/2}^{h/2}[D]\zeta^2 d\zeta\end{aligned}\right\} \tag{21}$$

A complete set of field equations for the 23 independent variables $\{\dot{N}\}, \{\dot{M}\}, \dot{U}_\xi, \dot{U}_\theta, \dot{W}, \{\dot{\varepsilon}_m\}, \{\dot{\varkappa}\}, \dot{\Phi}_\xi, \dot{\Phi}_\theta, \{\dot{\sigma}\}, \{\dot{\sigma}^t\}, \{\dot{N}^t\}$ and $\{\dot{M}^t\}$ is now given by the 23 equations (9), (11)$\sim$(13), (16), (17), (19) and (20).

3. Nondimensional Equations

In order to analyze the problem of shells under arbitrary unsymmetrical loads, the distributed loads, the ambient fluid temperature, the heat generation and the $(p+24)$ independent variables mentioned in section 2 are expanded into the Fourier series as follows.

$$\left.\begin{aligned}&\{T_j, \Theta_{\text{in}}, \Theta_{\text{out}}, Q_i\}\\ &=\frac{\sigma_0}{E_0\alpha_0}\sum_{n=0}^{\infty}\left\{\frac{t_j^{(n)}}{h^j}, \theta_{\text{in}}^{(n)}, \theta_{\text{out}}^{(n)}, \frac{\chi_0 h^i}{a}q_i^{(n)}\right\}\cos n\theta\\ &(i, j=0, 1, 2, \cdots, p)\\ &\{\dot{N}_\xi, \dot{N}_\theta, \dot{N}^t, \dot{M}_\xi, \dot{M}_\theta, \dot{M}^t\}\\ &=\sigma_0 h\sum_{n=0}^{\infty}\left\{\dot{n}_\xi^{(n)}, \dot{n}_\theta^{(n)}, \dot{n}^{t(n)}, \frac{h^2}{a}\dot{m}_\xi^{(n)},\right.\\ &\left.\frac{h^2}{a}\dot{m}_\theta^{(n)}, \frac{h^2}{a}\dot{m}^{t(n)}\right\}\cos n\theta\\ &\{\dot{\bar{N}}_{\xi\theta}, \dot{\bar{M}}_{\xi\theta}\}=\sigma_0 h\sum_{n=1}^{\infty}\left\{\dot{\bar{n}}_{\xi\theta}^{(n)}, \frac{h^2}{a}\dot{\bar{m}}_{\xi\theta}^{(n)}\right\}\sin n\theta\\ &\{\dot{U}_\xi, \dot{W}, \dot{\varepsilon}_{\xi m}, \dot{\varepsilon}_{\theta m}, \dot{\varkappa}_\xi, \dot{\varkappa}_\theta, \dot{\Phi}_\xi\}=\frac{\sigma_0}{E_0}\\ &\times\sum_{n=0}^{\infty}\left\{a\dot{u}_\xi^{(n)}, a\dot{w}^{(n)}, \dot{e}_{\xi m}^{(n)}, \dot{e}_{\theta m}^{(n)}, \frac{\dot{k}_\xi^{(n)}}{a}, \frac{\dot{k}_\theta^{(n)}}{a}, \dot{\varphi}_\xi^{(n)}\right\}\\ &\times\cos n\theta\\ &\{\dot{U}_\theta, \dot{\varepsilon}_{\xi\theta m}, \dot{\varkappa}_{\xi\theta}, \dot{\Phi}_\theta\}\\ &=\frac{\sigma_0}{E_0}\sum_{n=1}^{\infty}\left\{a\dot{u}_\theta^{(n)}, \dot{e}_{\xi\theta m}^{(n)}, \frac{\dot{k}_{\xi\theta}^{(n)}}{a}, \dot{\varphi}_\theta^{(n)}\right\}\sin n\theta\\ &\{\dot{\sigma}_\xi, \dot{\sigma}_\theta, \dot{\sigma}^t, \dot{P}_\xi, \dot{P}_\zeta\}\\ &=\sigma_0\sum_{n=0}^{\infty}\left\{\dot{s}_\xi^{(n)}, \dot{s}_\theta^{(n)}, \dot{s}^{t(n)}, \frac{h}{a}\dot{p}_\xi^{(n)}, \frac{h}{a}\dot{p}_\zeta^{(n)}\right\}\cos n\theta\\ &\{\dot{\sigma}_{\xi\theta}, \dot{P}_\theta\}=\sigma_0\sum_{n=1}^{\infty}\left\{\dot{s}_{\xi\theta}^{(n)}, \frac{h}{a}\dot{p}_\theta^{(n)}\right\}\sin n\theta\end{aligned}\right\} \tag{22}$$

where σ_0, E_0 and α_0 are a reference stress, a reference Young's modulus and a reference thermal expansion coefficient, respectively. And χ_0 is a reference thermal diffusivity $(=\lambda_0/(c_0\rho_0)$, λ_0: a coefficient of reference thermal conductivity, c_0: a reference specific heat, ρ_0: a reference mass density).

It should be noted that the Fourier expansions, Eqs. (22), are not the most general that could exist. For full generality, these expansions should be augmented by the sine-additional series for the cosine series and by the cosine-additional series for the sine series.

Substituting these into the above fundamental equations, the equations among the Fourier coefficients relating to the variables are obtained. From the heat conduction equations, the simultaneous differential equations for the coefficients $t_j^{(n)}$ $(j=0, 1, 2, \cdots, p)$ can be obtained as

$$A_1 Y''+A_2 Y'+A_3 Y=A_4+A_5(\partial Y/\partial\tau) \tag{23}$$

where $Y=\{t_0^{(n)}, t_1^{(n)}, t_2^{(n)}, \cdots, t_p^{(n)}\}^T$ and $\tau=\chi_0 t/a^2$. $A_1\sim A_3$ are $(p+1)\times(p+1)$ matrices determined from k_{in}, k_{out} and the shell form. A_4 is a $(p+1)\times 1$ matrix determined from Θ_{in}, Θ_{out}, k_{in}, k_{out} and η. A_5 is a $(p+1)\times(p+1)$ constant matrix.

Similarly eliminating the variables from the thermal deformation equations, the simultaneous differential equations for the displacement rates $\dot{u}_\xi^{(n)}$, $\dot{u}_\theta^{(n)}$, $\dot{w}^{(n)}$ and the bending moment rate $\dot{m}_\xi^{(n)}$ can be derived as

$$B_1 Z''+B_2 Z'+B_3 Z=B_4 \tag{24}$$

where $Z=\{\dot{u}_\xi^{(n)}, \dot{u}_\theta^{(n)}, \dot{w}^{(n)}, \dot{m}_\xi^{(n)}\}^T$. $B_1\sim B_3$ are 4×4 matrices determined from the shell form and ν. B_4 is a 4×1 matrix determined from the distributed loads and the temperature rise in addition to the shell geometries.

The integrations are carried out numerically using Simpson's 1/3 rule.

4. Numerical Method

A finite difference method is employed for the solutions of the two second order simultaneous differential equations (23) and (24). The usual central difference formulas are used for every mesh point except the discontinuity points and the boundary points of the shell. For the discontinuity points and the boundary points, forward and backward difference equations are employed. The derivatives with respect to time in Eq. (23) are treated by the Crank-Nicolson method. The solutions at any time are obtained by a summation of the incremental values due to the time increment.

5. Numerical Example

As numerical examples, functionally graded cylindrical shells composed of SUS 304 and ZrO_2 subjected to thermal loads due to fluid, which are expressed by step function in regard of time, are treated and two problems are analyzed.

By using a parameter V_S which denotes the volumetric ratio of SUS 304, four kinds of compositional distribution profiles with respect to relative thickness coordinate, ζ/h, are selected for the numerical examples as follows (Fig. 2)

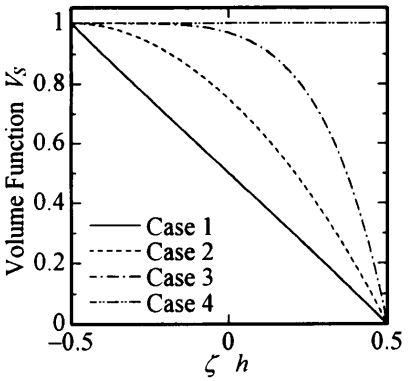

Fig. 2 Volumetric distribution of SUS 304 through thickness

$$\left.\begin{aligned}&\text{Case 1}: V_S=1-(\zeta/h+0.5)\\&\text{Case 2}: V_S=1-(\zeta/h+0.5)^2\\&\text{Case 3}: V_S=1-(\zeta/h+0.5)^5\\&\text{Case 4}: V_S=1\end{aligned}\right\} \quad (25)$$

Namely, case 1~case 3 represent the FGM shells whose outer and inner surfaces consist of ZrO_2 only and SUS 304 only, respectively, and case 1 shows that the volumetric ratio of SUS 304 varies lineally through shell thickness. Case 4 corresponds to the homogeneous shell made of SUS 304.

The material constants of SUS 304 and ZrO_2 employed in the calculations are as follows.

○ SUS 304

$$\left.\begin{aligned}&E=170\ \text{GPa},\ \nu=0.3\\&\rho=7.8\ \text{g/cm}^3,\ \lambda=19\ \text{W/(m·°C)}\\&c=0.56\ \text{kJ/(kg·°C)},\ \alpha=18\times10^{-6}\ 1/°\text{C}\end{aligned}\right\} \quad (26)$$

○ ZrO_2

$$\left.\begin{aligned}&E=210\ \text{GPa},\ \nu=0.32,\\&\rho=5.9\ \text{g/cm}^3,\ \lambda=3\ \text{W/(m·°C)}\\&c=0.3\ \text{kJ/(kg·°C)},\ \alpha=10\times10^{-6}\ 1/°\text{C}\end{aligned}\right\} \quad (27)$$

In the present calculation, six kinds of material constants in Eqs.(26) and (27) are assumed to be linearly dependent on the volume function V_S. For example Young's modulus $E(\zeta)$ is given as

$$E(\zeta)=E_Z\{1-V_S(\zeta)\}+E_S V_S(\zeta) \quad (28)$$

where E_S and E_Z are Young's modulus of SUS 304 and ZrO_2, respectively.

In the following two numerical examples, $\bar{T}_0$ and Θ_{in} are both 0°C, and K_{in} and K_{out} on inner and outer surfaces of the shell are both 3 kW/(m²°C). σ_0 has been selected as $\sigma_0=1$. The number of division through the thickness is chosen to be 19 for integration of thermal stress in Eqs.(20). On the other hand for integration of material constants in Eqs.(7) and (21), division number depends on the degree of temperature distribution polynomial, and the maximum number of 64 is selected here. The increment of time Δt is selected as 0.1 second, and the number of mesh points is chosen to be 51 for the half span of the

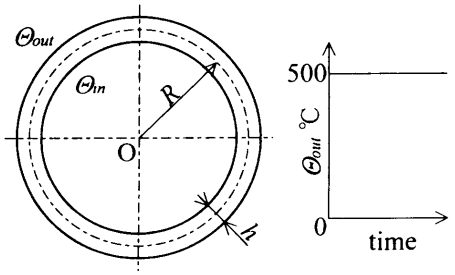

h = 10 mm R = 200 mm
Θ_{in} = 0 ℃ $\bar{T}_0$ = 0 ℃
K_{out} = K_{in} = 3 kW/(m²℃)

Fig. 3 Numerical example 1

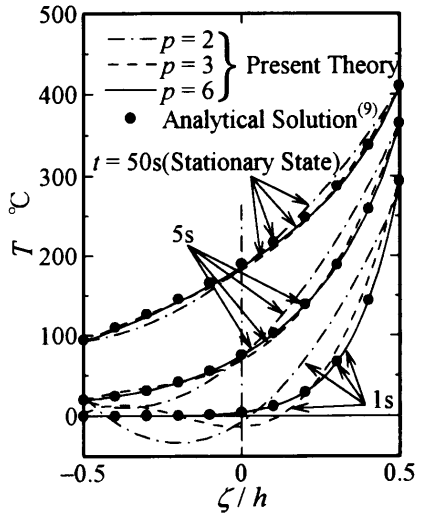

Fig. 4 Temperature distributions through thickness

cylindrical shells in example 2. These values are chosen with consideration of the convergence of the solutions, the capacity of the computer and computing time.

5.1 Example 1: Thermal analysis and evaluation of solution

A long cylindrical shell under axisymmetric thermal loading, where the compositional distribution profile through thickness is linear(case 1), is treated (Fig. 3), and the temperature distributions obtained are compared with solutions by other methods.

The variations of temperature distribution through shell thickness with time are shown in Fig. 4. In the figure, solid circles indicate the analytical solutions treated as multilayered composite cylinder(20 layers)by Tanigawa et al.[9]. The results from the present theory, whose temperature distributions through thickness are assumed to be the curves of the second, third and sixth orders, are plotted by chain lines, broken lines and solid lines, respectively. Just after thermal loading(t=1 second), using higher order curve of the temperature distribution in Eq.(4),

present solutions rapidly converge with p to the analytical solutions. Therefore it is found that the present method is effective for the analysis of FGM shells.

5.2 Example 2: Thermal stress analysis

The simply supported cylindrical shells subjected to locally distributed axisymmetric thermal loading due to fluid are analyzed (Fig. 5). For four kinds of compositional distribution profiles (case 1~case 4) suitable degrees p of temperature distribution polynomial are 6, 8, 10 and 4, respectively. The boundary conditions at both ends are assumed to be adiabatic.

Now we shall discuss some results of calculations. In Figs. 6~15, except Figs. 8 and 11, the solid lines, broken lines and two kinds of chain lines indicate the values for four cases of compositional distribution profiles, respectively.

The variations of temperature distribution through the thickness at point C ($\xi=0.5$) of the shell

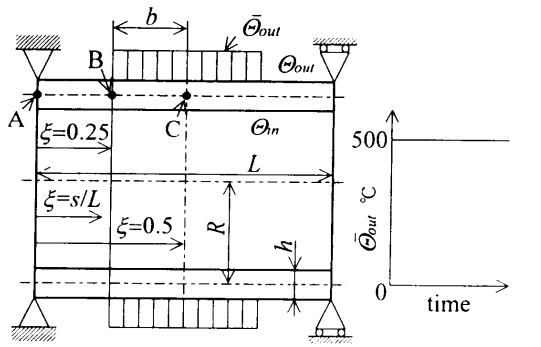

L = 600 mm R = 200 mm
h = 10 mm b = 150 mm
Θ_{in} = 0 ℃ $\bar{T}_0$ = 0 ℃
$K_{out} = K_{in}$ = 3 kW/(m²℃)

$$\Theta_{out} = \begin{cases} 0\ ℃ (0 \le \xi < 0.25) \\ \bar{\Theta}_{out} (0.25 \le \xi \le 0.5) \end{cases}$$

Fig. 5 Numerical example 2

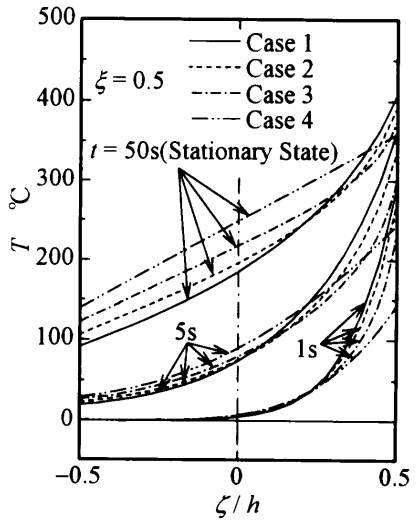

Fig. 6 Temperature distributions through thickness at point C

are shown in Fig. 6. Figure 7 illustrates the variations with time of temperature at point C on the inner and outer surfaces of the shell, and Fig. 8 gives the meridional distributions of temperature on the surfaces in the case 1. Just after thermal load is applied, the temperature near the heated surface rises quickly, and the temperature near the inner surface rises gradually. After about 50 seconds the temperature becomes the steady state, however, the difference of temperature between inner and outer surfaces is still large. Because of smaller thermal conductivity coefficient of ZrO_2 than one of SUS 304, with the increased volumetric ratio of ZrO_2, this difference of temperature becomes remarkable. Excepting the region near the outer surface of the shell, the temperature in the homogeneous shell of SUS 304 on the steady state is high in comparison with one in the FGM shells, and shows the linear distribution through thickness. The meridional distribution of temperature in other cases (case 2~case 4), not illustrated here, is almost the same as one in Fig. 8. Because the thickness of the shell is small compared with other dimensions, and the parameters k_{in} and k_{out} using in this example are relatively large, temperature distributions along the meridian change stepwise near the heating boundary (at point B: $\xi=0.25$), and except the heating region

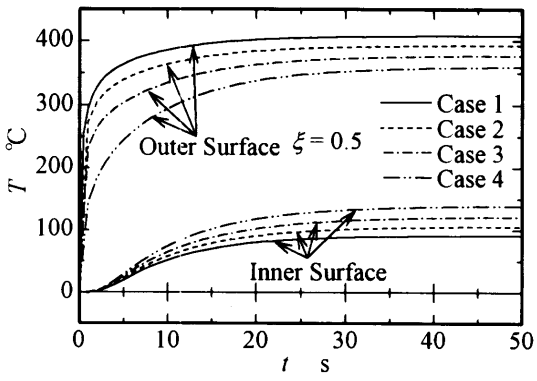

Fig. 7 Variations of temperature at point C with time

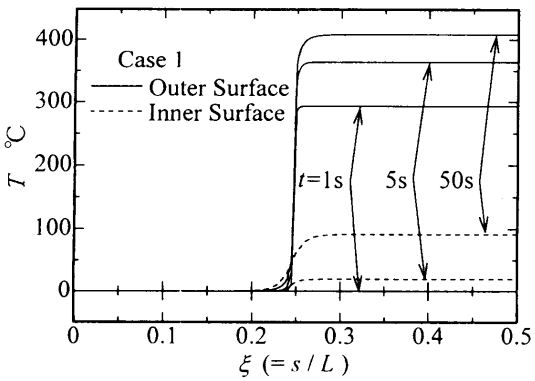

Fig. 8 Meridional distributions of temperature (Case 1)

(ξ=0.25～0.5) initial temperature is maintained.

In Fig. 9 the variations of circumferential stress distribution through the thickness at point C are shown, and in Fig. 10 the variations of σ_θ on the inner and outer surfaces at point C with time are illustrated. The aspect of variations of meridional stress σ_ξ, not illustrated here, is almost the same as one of variations of σ_θ. Near the heated surface of the shells, due to the remarkable temperature gradient through shell thickness, high compressive stresses arise, and the stresses become large with the increased volumetric ratio of ZrO_2. Subsequently the stresses reverse largely with the increase of thermal deformation due to heat conduction(cf. Fig. 12), but compressive stress states are still maintained in steady state in all shells. On the other hand, near the inner surface of the shell, just after thermal loading, tensile stresses occur and then gradually increase. Those increments in the FGM shells become large with the increased volumetric ratio of SUS 304. In comparison with FGM shells, homogeneous shell(case 4) of SUS 304 gives higher tensile stress distributions on inner side of the shell. Considering with the fact that in steady state compressive stresses are maintained near the outer surface of FGM shells, the advantage of FGM shells, which arrange metals and ceramics in the lower and higher temperature portions, respectively, is recognized.

Moreover, Fig. 11 shows the meridional distributions of σ_θ on inner and outer surfaces of the shell in case 1. Near the point B on outer surface, where the temperature gradient along the meridian becomes large, meridional variations of σ_θ also appear large.

Figure 12 shows the variations with time of meridional displacement U_ξ at point A (ξ=0) and radial displacement W at point C. In Fig. 13, the meridional distributions of displacements U_ξ and W are illustrated. After thermal load is applied, both displacements increase gradually until the steady state (t=50 sec), but deformed area is restricted to the heated region. Because of larger thermal expansion coefficient of SUS 304 than one of ZrO_2, deformation becomes large with the increased volumetric ratio of SUS 304.

Finally the meridional distributions of resultant stress N_θ and resultant moment M_ξ are depicted in

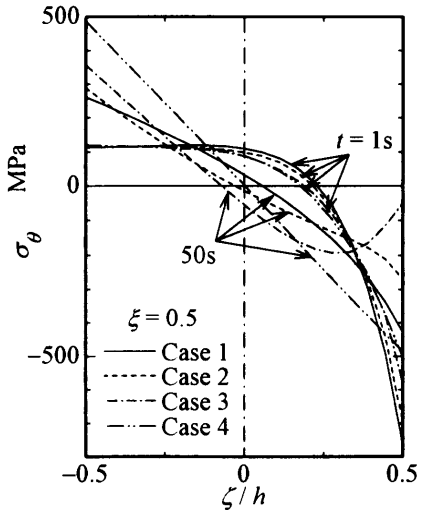

Fig. 9 Distributions of stress σ_θ through thickness at point C

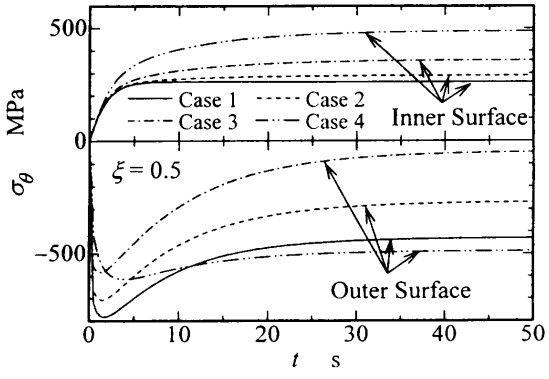

Fig. 10 Variations of stress σ_θ on inner and outer surfaces at point C with time

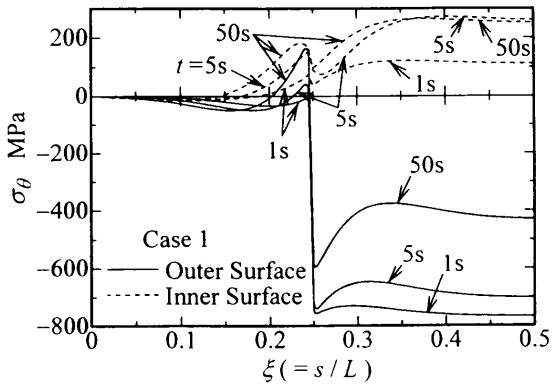

Fig. 11 Meridional distributions of stress σ_θ (Case 1)

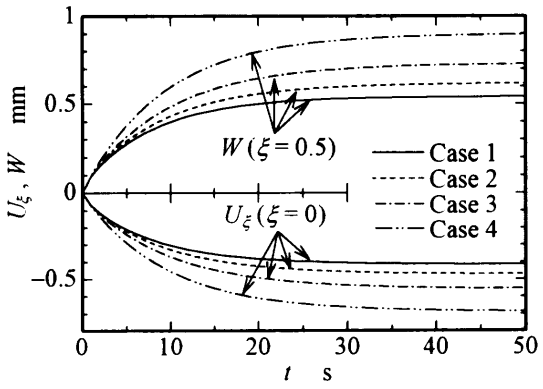

Fig. 12 Variations of displacements U_ξ and W with time

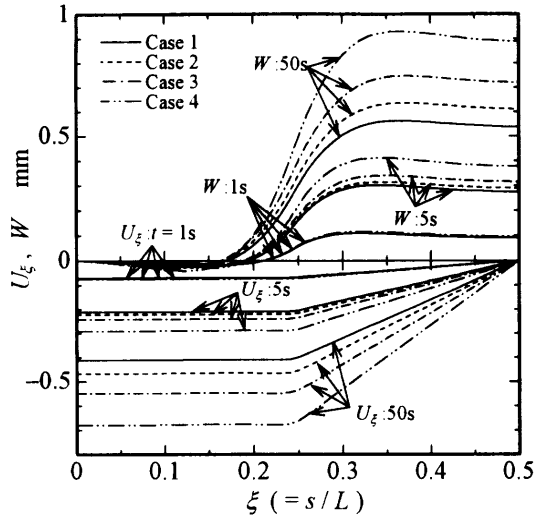

Fig. 13 Meridional distributions of displacements U_ξ and W

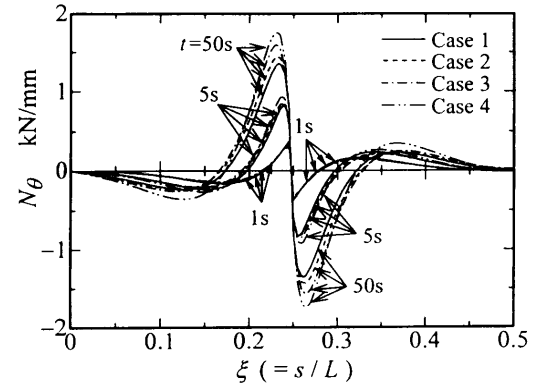

Fig. 14 Meridional distributions of resultant force N_θ

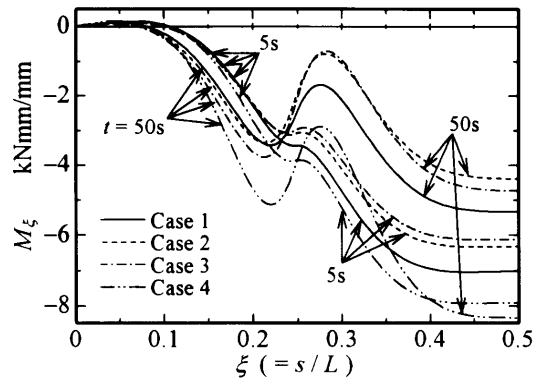

Fig. 15 Meridional distributions of resultant moment M_ξ

Figs. 14 and 15, respectively. Near point B, where the gradient of temperature along the meridian is very large, meridional variations of N_θ appear remarkable. These variations become large with the increased volumetric ratio of SUS 304. N_θ increases with time monotonically as well as the meridional distributions of W with time. On the other hand, in FGM shells M_ξ decreases on the heated region, but in the homogeneous shell, M_ξ shows little variation.

6. Conclusions

In this paper we have described the numerical analysis of the thermal stress and deformation for axisymmetrical thin shells of functionally graded material subjected to thermal loads due to fluid. In order to improve the accuracy of the solutions, the temperature distribution through the thickness has been assumed to be a curve of high order, and the equations of heat conduction and heat transfer have been solved under appropriate initial and boundary conditions. Suitable degree of temperature distribution polynomial has been determined from evaluation of convergency of the solutions according to variation of the degree. By using the temperature distributions obtained, the stresses and deformations have been calculated from the thermal stress equations. The equations of equilibrium and the strain displacement relations have been derived from the Sanders thin shell theory. The numerical method selected for this problem is a method using finite difference in both space and time.

As numerical examples, functionally graded cylindrical shells composed of SUS 304 and ZrO_2 subjected to thermal loads due to fluid, which are expressed by step function in regard of time, have been analyzed. First we have analyzed the heat conduction problem of the long shell under axisymmetric thermal loading. The obtained temperature distributions have been compared with ones by other methods, and the accuracy of the solutions has been evaluated. Secondly we have analyzed the simply supported cylindrical shells subjected to locally distributed axisymmetric thermal loading, and have compared the solutions for various compositional distribution profiles in FGM.

From the computations, we found the following.

(1) Using higher order curve of the temperature distribution, we can expect to obtain more accurate solutions for the problems where the locally large gradient of temperature distribution through shell thickness occurs in FGM shells. Therefore the present method is effective in the analysis of FGM shells.

(2) With the increase of ZrO_2, which has small thermal conductivity, the temperature on the heating surface becomes higher and on the opposite surface lower, and the temperature gradient through the thickness becomes large at the stationary state. Also the stress distribution and the deformation vary significantly depending on the compositional distribution profiles in FGM.

References

(1) Fukui, Y., Yamanaka, N. and Wakashima, K., The Stresses and Strains in a Thick-Walled Tube of Functionally Gradient Material under Uniform Thermal Loading, Trans. Jpn. Soc. Mech. Eng.,(in Japanese), Vol. 58, No. 546, A(1992), p. 257.

(2) Sumi, N. and Ito, Y., The Propagation and Reflection of Thermal Stress Waves in Anisotropic Nonhomogeneous Hollow Cylinders and Spheres, Nucl. Eng. and Design, Vol. 140, No. 2(1993), p. 133.

(3) Tanaka, K., Tanaka, Y., Watanabe, H, Poterasu, V. F. and Sugano, Y., An Improved Solution to Thermoelastic Material Design in Functionally Gradient Materials: Scheme to Reduce Thermal Stresses, Computer Methods in Apl. Mech. and Eng., Vol. 109(1993), p. 377.

(4) Obata, Y. and Noda N., Steady Thermal Stresses in a Hollow Circular Cylinder and a Hollow Sphere of a Functionally Gradient Material, J. Thermal Stresses, Vol. 17, No. 3(1994), p. 471.

(5) Ishikawa, T., Thermal Deformation and Thermal Stress of FGM Plates under Steadily Gradient Temperature Field, Proc. 1st Int. Symp. on FGM, Sendai, Japan(1990), p. 11.

(6) Sugano, Y., Morishita, H. and Tanaka, K., An Analytical Solution for Transient Thermal Stress in a Functionally Gradient Plate with Arbitrary Nonhomogeneities and Thermal Boundary Conditions.(Material Properties Determined by Fuzzy Inference), Trans. Jpn. Soc. Mech. Eng.,(in Japanese), Vol. 59, No. 567, A(1993), p. 2666.

(7) Ishizuka, T. and Wakashima, K., Residual Thermal Stresses in Ceramic/Metal Functionally Gradient Material Plates, Trans. Jpn. Soc. Mech. Eng.,(in Japanese), Vol. 60, No. 571, A(1994), p. 748.

(8) Ootao, Y., Akai, T. and Tanigawa, Y., Three-Dimensional Transient Thermal Stress Analysis of a Nonhomogeneous Hollow Circular Cylinder due to a Moving Heat Source in the Axial Direction, J. Thermal Stresses, Vol. 18, No. 5(1995), p. 497.

(9) Tanigawa, Y., Fukuda, T., Ootao, Y. and Tanimura, S., Transient Thermal Stress Analysis of a Multilayered Composite Laminate Cylinder with a Uniformly Distributed Heat Supply and [Its Analytical Development to Nonhomogeneous Materials], Trans. Jpn. Soc. Mech. Eng., (in Japanese), Vol. 55, No. 513, A(1989), p. 1133.

(10) Sanders, J. L., Jr., An Improved First-Approximation Theory for Thin Shells, NASA Tech. Rep., R-24(1959), p. 1.

(11) Takezono, S., Tao, K., Aoki, T. and Inamura, E., Elasto/Visco-Plastic Deformation of Shells of Revolution under Thermal Loading due to Fluid, JSME Int. J., Ser. A, Vol. 38, No. 2(1995), p. 185.

(12) Takezono, S., Tao, K., Aoki, T. and Inamura, E., Elasto/Visco-Plastic Deformation of Moderately Thick Shells of Revolution under Thermal Loading due to Fluid, Trans. 12th Int. Conf. Struct. Mech. in Reactor Technol., Vol. L(1993), p. 257.

(13) Takezono, S., Tao, K. and Inamura, E., Elasto/Visco-Plastic Deformation of Multi-Layered Shells of Revolution under Thermal Loading due to Fluid, Pressure Vessels and Piping, Vol. 302, Composites for the Pressure Vessel Industry, ASME(1995), p. 223.